Effects of ultraviolet and vacuum ultraviolet synchrotron radiation on organic underlayers to modulate line-edge roughness of fine-pitch poly-silicon patterns

Hiroyuki Miyazoe, , Sebastian U. Engelmann, and , Michael A. Guillorn, Dongfei Pei, , Weiyi Li, , Jason L. Lauer, and , J. Leon Shohet, and Nicholas C. M. Fuller

Citation: Journal of Vacuum Science & Technology A: Vacuum, Surfaces, and Films **35**, 05C306 (2017); doi: 10.1116/1.4985541

View online: http://dx.doi.org/10.1116/1.4985541

View Table of Contents: http://avs.scitation.org/toc/jva/35/5

Published by the American Vacuum Society

Effects of ultraviolet and vacuum ultraviolet synchrotron radiation on organic underlayers to modulate line-edge roughness of fine-pitch poly-silicon patterns

Hiroyuki Miyazoe,[a] Sebastian U. Engelmann, and Michael A. Guillorn
IBM T.J. Watson Research Center, 1101 Kitchawan Rd., Yorktown Heights, New York 10598

Dongfei Pei, Weiyi Li, Jason L. Lauer, and J. Leon Shohet
Plasma Processing and Technology Laboratory and Department of Electrical and Computer Engineering, University of Wisconsin-Madison, Madison, Wisconsin 53706

Nicholas C. M. Fuller
IBM T.J. Watson Research Center, 1101 Kitchawan Rd., Yorktown Heights, New York 10598

(Received 3 April 2017; accepted 17 May 2017; published 13 June 2017)

Deformation of the pattern or the increase in line roughness during plasma etching becomes more significant with the shrink of complementary metal–oxide–semiconductor patterns. For aggressively scaled patternings, an organic underlayer (UL) is often used under the photoresist and a thin layer of a Si-containing hardmask. In this work, the effect of ultraviolet/vacuum ultraviolet (VUV) photons on UL parameters such as wavelength, photon dose, and process order was investigated using synchrotron radiation. First, the index of refraction and extinction coefficients of mask materials such as e-beam resist [hydrogen silsesquioxane (HSQ)] and organic UL (NFC-1400; NFC) were measured by utilizing the Kramers–Kronig relations and/or ellipsometry measurements depending on the wavelength involved. Second, VUV photons at specific wavelengths, corresponding to absorption maxima of HSQ and NFC at 54 nm (HSQ), 62 nm (HSQ and NFC), 88 nm (HSQ), 112 nm (NFC), 138 nm (HSQ), 155 nm (NFC), 194 nm (NFC), and 238 nm (NFC), were exposed before or/and after etching of NFC. The authors continued to etch into poly-Si, and the resulting line-edge roughness (LER) was measured. The improvement of the LER was seen at the wavelengths corresponding to the absorption maxima of NFC, and the degree of LER improvement was better at the higher photon dose up to 3×10^{17} photons/cm^2. The LER reduced from 6.7 to 4.2 nm and to 3.6 nm when the VUV photons at wavelengths of 62 and 155 nm, respectively, were used for exposure. In contrast, pattern degradation was observed at the wavelengths corresponding to the absorption maxima of HSQ. These findings indicate that optimizing VUV radiation corresponding to the UL materials greatly influences the LER. © *2017 American Vacuum Society*. [http://dx.doi.org/10.1116/1.4985541]

I. INTRODUCTION

As the feature size of ultra-large-scale integrated circuit devices has become smaller, the control of line edge roughness (LER) becomes very critical for device performance. This can be due to fluctuations of threshold voltage and on- and off-current variations in MOSFETs (Refs. 1 and 2) and the increase in line resistivity of copper interconnects.[3] To improve the etch budget for photoresist materials, patterning of CMOS materials with 80-nm pitch and beyond typically requires a trilayer patterning scheme, which consists of a thin resist, spin-on glass/SiO, and an organic underlayer (UL).[4,5] The UL, such as organic planarizing layers and spin-on carbon and/or vapor-deposited carbon layers, plays an important role in pattern transfer.

During the pattern transfer of aggressively scaled pitches, deformation of the initial lithographic pattern in the PR material is often observed.[6,7] Patterning of the subsequent spin-on glass/SiO_2 and UL has typically not shown any deformation. Deformation is usually observed during the transfer from the UL into Si or dielectric materials. This deformation and the impact on the LER of fabricated devices are significant challenges to overcome during patterning at aggressively scaled dimensions. Electron-beam (e-beam) lithography has also been used for device prototyping at dimensions unobtainable with state-of-the-art optical lithography.[8] The same aforementioned deformation phenomenon of the UL material has been observed.[9,10] The mechanism of pattern deformation has also been shown to be due to a local expansion of a fluoridated PR (Refs. 6 and 7) or a thermal expansion of surface deposits consisting of carbon fluoride[11] and the formation of a high tensile-stress-induced layer (~5 nm thick) by the irradiation of oxygen and fluorine radicals.[12,13]

The degree of pattern deformation can be improved by thermal treatment of the UL material at higher temperature, decreasing ion energy,[11] lowering the substrate temperature during etch,[11] reducing the hydrogen content in UL materials,[9] and/or reducing the O_2 gas flow ratio or using an O_2 free plasma chemistry for UL etch.[14] Another attractive approach to reduce line roughness of patterned lines has been a plasma pretreatment of the organic materials, such as the photoresists and ULs. The impact of plasma pretreatment on a 193-nm photoresist has been intensively studied using

[a]Electronic mail: miyazoe@us.ibm.com

HBr,[15–19] HBr/O_2,[20] Ar,[15,16] H_2,[15] Cl_2,[15] and He (Refs. 21 and 22) plasmas. In the case of HBr plasma treatment, resist modification may be due to synergistic effects between the ions and the vacuum ultraviolet (VUV) photons[23] and/or between Br radicals and VUV photons.[17] Plasma treatment of organic ULs has also been investigated by a few groups.[24] Ono *et al.*[24] reported that the improvement of line wiggling with H_2 plasma-treated organic UL was attributed to the formation of diamondlike amorphous carbon up to a depth of approximately 50 nm. Our group also reported that He plasma treatment on an organic UL material is effective to reduce line roughness.[14,25] One possible reason for roughness smoothing with He plasma treatment is that a He plasma has strong VUV photon emission at a wavelength of 58.4 nm (21.2 eV).[26] However, the mechanism of this roughness smoothing effect is not well known.

In this work, the effect of the VUV photons on poly-Si etching using the above-mentioned trilayer scheme is investigated using synchrotron radiation in order to unveil the mechanism of the VUV photon exposure on the improvement of line roughness. To accomplish this, the index of refraction and the extinction coefficient of the electron-beam resist and the organic UL are measured using synchrotron radiation in the VUV range (50–150 nm) and ellipsometry in the UV to visible range (150–800 nm). Based on the optical-measurement results, specific wavelengths for photon exposure to the target patterns were chosen. The photon dose, photon flux, and process order were varied as parameters.

II. EXPERIMENT

A. Setup for the refraction and extinction coefficient measurement

The index of refraction (n) and the extinction coefficient (k) in the visible, UV, and VUV range of dielectric films were measured using two different methods depending on the photon wavelength. In the visible and UV range (150–800 nm or 1.5–8 eV), they were measured using a variable-angle spectroscopic ellipsometer (J.A. Woolam VUV-VASE ellipsometer, VU-302). In the VUV range (50–150 nm, or 8–25 eV), these were extracted by using the Kramers–Kronig relations from a combination of reflectance measurements including the ellipsometric measurements in the longer-wavelength range. The reflectance measurements were made at the Synchrotron Radiation Center at the University of Wisconsin-Madison.

In principle, the reflectance of the film can be measured from 5 to 25 eV in a synchrotron. However, at lower photon energies (longer wavelengths), the light reflected from the interface between the film and the substrate will interfere with that reflected from the surface of the film. As a result, the measured reflectance at lower energy is a combination of the reflectance at the film surface and that of the interface of the film with the substrate. At higher energies (larger than 10 eV), the photon absorption of most materials becomes very strong and the penetration depth of the photons is usually less than 100 nm. If the film thickness is much larger than the penetration depth, there will be very little reflected light from the substrate interface. Therefore, accurate reflectance measurements of the material could be measured from 10 to 25 eV.

The detail of the reflectometer setup has been shown elsewhere.[27] The reflectometer setup consists of four parts: (1) a 90% transparent nickel mesh, (2) a grounded sample mount, (3) a linear translator, and (4) a picoammeter connected to the nickel mesh. The nickel mesh and the sample mount are connected to the linear translator and placed inside a vacuum chamber. The vacuum chamber is connected to the synchrotron photon source. When the VUV photons are normally incident on the nickel mesh, ten percent are absorbed by the mesh, the majority of which results in photoemission of electrons. To maintain charge neutrality, the same number of electrons flows from the ground to the nickel mesh. This current, which is equivalent to the photoemission current, is measured using a Keithley-486 picoammeter. To improve the accuracy of measurements, the nickel mesh was negatively biased, which prevents electrons in the chamber, e.g., those photoemitted from the sample or other objects, from being collected by the nickel mesh.

It should be noted that the reflectance is inversely proportional to the absorbance of photons. In this work, it was decided that the most accurate relationship could be found by measuring the substrate current during irradiation.[27] This method has a number of advantages. First, the substrate current measured is proportional to the total number of photoemitted electrons regardless of the angle of emission, and so, it is not necessary to angle-resolve the photoemission flux. Since the ellipsometer measurements are true optical reflectance measurements and the substrate–current measurements can be made to match the ellipsometer measurements in the regions where they overlap, it is apparent that the data are consistent.

To calibrate the system, the nickel mesh current was measured under two conditions (1) when the sample was present and (2) when the sample was absent. When the sample was absent, a photon dump was used to minimize any possible reflection from the walls of the chamber. Thus, the net photon flux incident on the nickel mesh when the sample was absent should only be that due to the source photon flux. Under these circumstances, the reading from the picoammeter (I_0) is proportional to the source photon flux.

When the sample was present, the nickel mesh is subjected to two photon fluxes: (1) the source photon flux and (2) the photon flux that is reflected from the sample. The fraction of photons reflected at a given energy is directly related to the reflectance of the material at that energy. Thus, the measured mesh current (I_1) should be proportional to the sum of the source photon flux and the reflected photon flux. It should be noted that the incident photon flux passing through the mesh is reduced by a factor that depends on the transparency of the nickel mesh. In this case, the transparency is 90%. This will be taken into account in the reflectance calculations.

Combining the two measured mesh currents and the known transparency coefficient of the mesh, the following

expression can be used to calculate the reflectance of the sample

$$R = \frac{I_1 - I_0}{\tau I_0}, \quad (1)$$

where R is the reflectance, τ is the transparency of the mesh, I_0 is the nickel mesh current without the sample, and I_1 is the nickel mesh current when the sample is present. In this work, hydrogen silsesquioxane (HSQ; Dow Corning) and NFC-1400 (NFC; JSR) were used as an e-beam resist and an organic UL, respectively, and were measured using this method. However, this method can easily be extended to other materials.

B. Etching experiments

Sample preparation and etch experiments were performed at the IBM T.J. Watson Research Center. The VUV/UV exposures were carried out at the Synchrotron Radiation Center at the University of Wisconsin-Madison (UW-Madison). Fifty nanometer-thick poly-Si at a pitch of 50–80 nm was chosen as a test vehicle. Poly-Si was deposited on the 5-nm layer of SiO by chemical vapor deposition at 625 °C. The method of the e-beam based patterning is described elsewhere.[8] The organic UL, 75 nm-thick NFC-1400 (NFC; JSR), was spin-coated on the polysilicon at a spin speed of 4500 rpm and baked at 200 °C. An approximately 20-nm thick HSQ based electron-beam resist was coated on NFC at 3000 rpm. The structures of HSQ and NFC are illustrated in Figs. 1(a) and 1(b), respectively. The substrates were exposed to a focused electron beam using a Vistec VB6 operating at 100 keV with a pixel size of 5 nm. All exposures were performed using proximity-effect corrected patterns prepared using the method described by Rooks *et al.*[28] Typical feature doses ranged from 12 to 16 mC/cm^2. Consequently, a beam current of 10 nA was selected to enhance exposure throughput. Following exposure, the substrates were developed using a standard 0.26 N developer (OPD 7262, Fujifilm) for 4 min in a double puddle process on a conventional track coat and bake system (Mark 8, Tokyo Electron Limited).

An AMAT DPS232 Minos inductively coupled plasma etch tool was used for this work. The RF frequency was 13.56 MHz on both the top (source) and the bottom (bias). An electrostatic chuck maintained at 65 °C held the wafer in place. NFC was etched using a N_2-O_2-C_2H_4-Ar plasma for 29 s. The poly-Si etch process consisted of two steps: (1) etch step of native oxide using CF_4 and C_2H_4 plasmas for 5 s and (2) main etch step using HBr-O_2-He plasmas for 78 s. NFC was removed after poly-Si etch using an N_2-O_2 plasma ashing process for 60 s and cleaned with dilute hydrofluoric acid (100:1) solution using in/out dip.

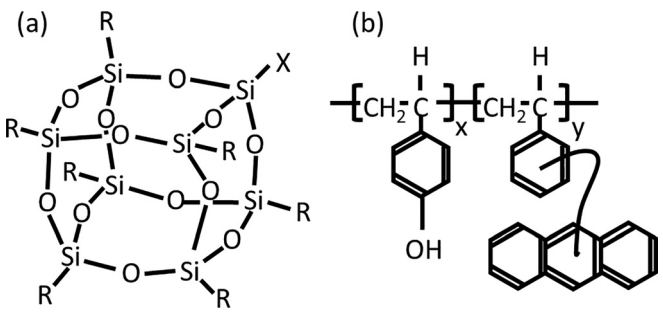

FIG. 1. Structures of (a) HSQ and (b) NFC.

The process flows used in this work are schematically summarized in Figs. 2(a)–2(d). Figure 2(a) presents our standard process flow without VUV exposure. As aforementioned, no significant pattern deformation was observed during the NFC etch. For the standard process without VUV treatment, the line critical dimension (CD) slightly decreased from 24.3 to 20.3 nm, while the LER remained almost the same (2.5 nm before NFC etch and 2.4 nm after). During poly-Si etch, line CD increased from 20.3 to 30.7 nm and the LER significantly increased from 2.4 to 6.7 nm. The wavelength of the VUV light (54–238 nm), dose (5×10^{14} and 3×10^{17} photon/cm^2), and ordering of the process were used as parameters. Figures 2(b) and 2(c) show the process flows for a single VUV exposure. Experimental samples were shipped to UW-Madison after the etching of NFC. After VUV exposure, the samples were then shipped back to IBM where the remainder of the process was completed [Fig. 2(b)]. VUV is shown in Fig. 2(b) before the poly-Si etch and in Fig. 2(c) before the NFC etch. In addition, two separate VUV exposures, before and after the NFC etch were performed with the results shown in Fig. 2(d).

The etched samples were characterized using a scanning electron microscope (SEM). CD, LER, and line width roughness data are measured using SUMMIT from the SuMMIT software Division of EUV Technology Corporation. Input SEM images have a maximum line length of 1024 pixels with a pixel size of 1.1 nm. The number of lines averaged for each measurement is the number of lines between a set of template lines. In this paper, the results are all for and 80-nm pitch unless otherwise mentioned.

III. RESULTS AND DISCUSSION

A. Measurement of the refractive index and extinction coefficient

The combined reflectance spectra of HSQ and NFC are shown in Fig. 3(c) together for each material used in this study. There is good agreement between both the low-energy region (hollow symbols are for less than 8 eV, calculated from n and k measured by ellipsometry) and the high-energy region (solid symbols are for greater than 8 eV, measured using the reflectometer in the synchrotron) for HSQ and NFC.

With the measured reflectance, it is possible to use the Kramers–Kronig relations, to obtain the phase difference of the electromagnetic wave after reflection, so as to obtain the n and k values. The equations used for this calculation are[27,29]

$$\theta(E) = \frac{1}{\pi}\int_0^\infty \ln\left|\frac{E' + E}{E' - E}\right| \frac{d \ln\sqrt{R(E')}}{dE'} dE', \quad (2)$$

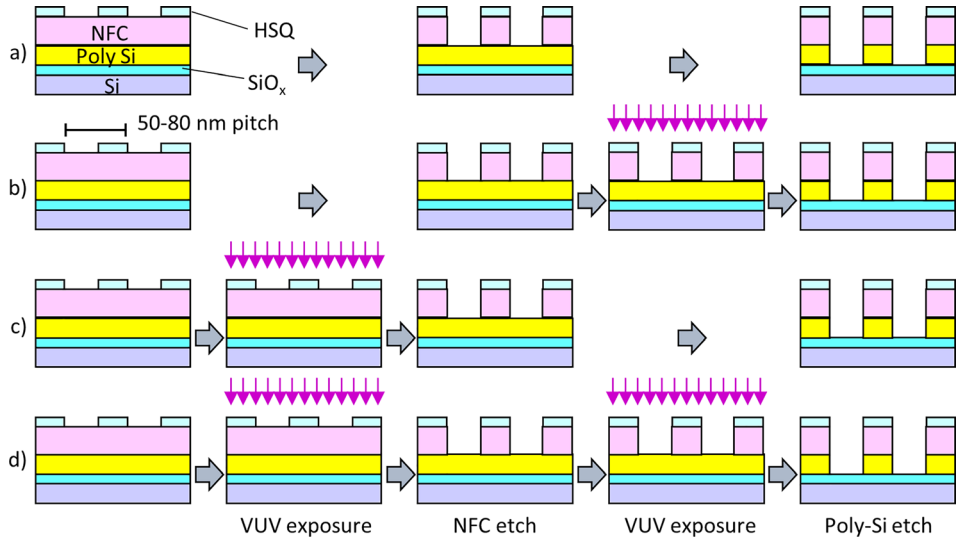

FIG. 2. (Color online) Process flow of (a) no VUV exposure, (b) single VUV exposure flow I (NFC etch => VUV exposure => poly etch), (c) single VUV exposure flow II (VUV exposure => NFC etch => poly etch), and (d) double-exposure flow (VUV exposure => NFC etch => VUV exposure => Poly etch).

$$n(E) = \frac{1 - R(E)}{1 + R(E) - 2\cos[\theta(E)]\sqrt{R(E)}}, \tag{3}$$

$$k(E) = \frac{2\sin[\theta(E)]\sqrt{R(E)}}{1 + R(E) - 2\cos[\theta(E)]\sqrt{R(E)}}, \tag{4}$$

where R is the reflectance at normal incidence, θ is the phase angle change of the reflection and E is the photon energy at which the index of refraction and the extinction coefficient are to be evaluated. It can be seen from the integration limits that an accurate calculation requires a measurement of the reflectance over the full spectrum. However, it is not possible to cover the whole spectrum from 0 to infinity. For values of E that are of interest, the largest contributions to the integral are from those regions that are near the singularity at the point at where $E' = E$ in Eq. (2). Thus, with a wide energy range of reflectance data measured especially near the singularity, reasonably accurate values of n and k can be calculated within that range.[30] In order to improve the accuracy, the ellipsometric values of n and k were converted into an equivalent reflectance to calculate corresponding reflectance in the visible and UV range, using the Fresnel equations under normal incidence conditions with the expression below,

$$R = \left|\frac{1 - (n + ik)}{1 + (n + ik)}\right|^2. \tag{5}$$

This calculated reflectance was then combined with the synchrotron-measured reflectance in the VUV range, thereby extending the range of integration. When performing the Kramers–Kronig integrations, the values of R outside of the range from the two measurements described above were set to be constant. The calculated n and k spectra are shown in Figs. 4(a) and 4(b), respectively. The extinction coefficient showed absorption maxima for NFC at 62 nm (20 eV), 112 nm (11 eV), 155 nm (8.1 eV), 193 nm (6.4 eV), 238 nm (5.2 eV), and 263 nm (4.7 eV) and for HSQ at 54 nm (23 eV), 62 nm (20 eV), 89 nm (14 eV), and 138 nm (9 eV).

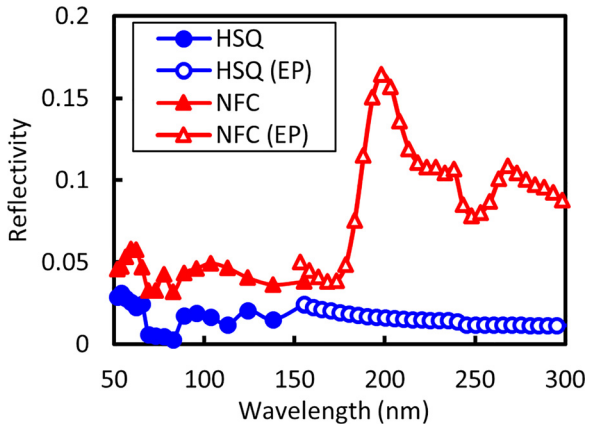

FIG. 3. (Color online) Reflectance vs wavelength. Solid points were measured with the synchrotron; hollow points were calculated from n and k that were measured using the ellipsometer. EP stands for the ellipsometer.

B. Poly-Si etch experiment

VUV light with wavelengths at absorption maxima in n and k measurements was exposed to the line space patterns before NFC etching [see Fig. 2(c)]. Line CD and LER values after poly-Si etch are plotted in Figs. 5(a) and 5(b), respectively. We exposed VUV light at 54 nm (HSQ), 62 nm (HSQ and NFC), 77 nm, 88 nm (HSQ), 112 nm (NFC), 138 nm (HSQ), 155 nm (NFC), 194 nm (NFC), and 238 nm (NFC). Line CD and LER values for post-e-beam lithography (dotted line) and non-VUV-treated patterns (solid line) are also drawn as a reference. For wavelengths shorter than 155 nm, a VUV photon dose of 3×10^{17} photons/cm^2 was used. For wavelengths longer than 155 nm, a fluence of 5×10^{14} photons/cm^2 was used. The difference in the photon dose is attributed to the fact that the photon flux at the longer

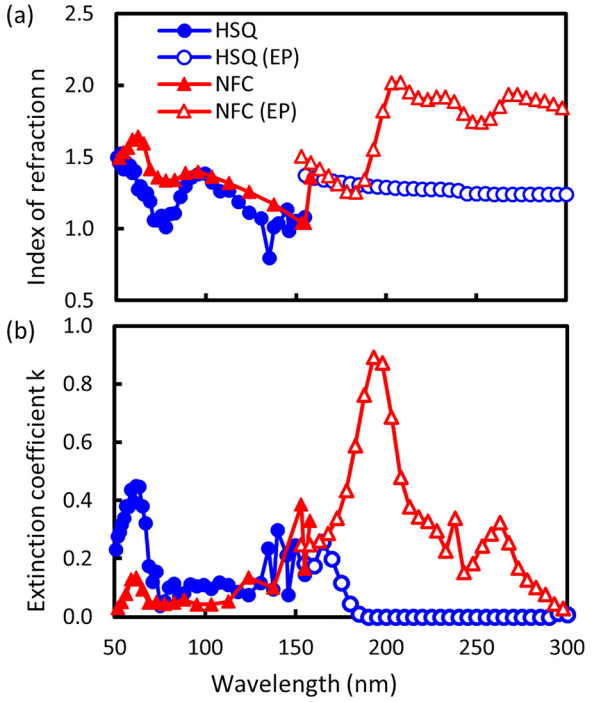

FIG. 4. (Color online) Calculated (a) index of refraction n and (b) extinction coefficient k. Solid points were calculated from the Kramers–Kronig relations; hollow points were measured using the ellipsometer. EP stands for the ellipsometer. All data are plotted with the same x axis (wavelength).

wavelengths was much lower. We did not see any significant correlation in VUV wavelength between line CDs and absorption maxima. The line CD that was measured after a photon dose of 3×10^{17} photons/cm^2 was larger than that of post-e-beam lithography (24.3 nm) and independent of exposed wavelength. The line CD after an exposure of a fluence of 5×10^{14} photons/cm^2 resulted in a smaller CD than that for the pristine (unexposed) case. LER measurements also showed some dependence on the wavelength. Improvement of LER is seen at VUV wavelengths of 155 nm at a photon dose of 3×10^{17} photons/cm^2, resulting in 4.2 nm compared with the non-VUV exposed case (LER = 6.7 nm). This wavelength corresponds to the desorption maxima of NFC [Fig. 4(b)]. The wavelength of 62 nm also showed relatively low LER (7.5 nm) compared to other wavelengths. This wavelength corresponds to the absorption maxima of HSQ and NFC (Fig. 4). Based on the result at 155 nm comparing the photon doses, LER might have improved at 193 and 238 nm at a higher dose; however, the experiments at high dose conditions were not conducted because of the lower synchrotron flux at these wavelengths. At the wavelengths of 54 (HSQ) and 138 nm (HSQ), significant pattern deformation is observed as shown in Fig. 6. HSQ is known as a low dielectric-constant material for lowering the capacitance between interconnect metal wiring[31] and a negative-tone resist for e-beam lithography. Many reports have been published on the damage to low-k materials by VUV photons, which includes breakage of chemical bonds and the formation of a weakened SiO_2-like structure within the photon-penetrated layer.[32] The pattern degradation at the wavelengths at 54 and 138 nm is probably attributed to this mechanism.

Since we observed relatively low LER at 62 and 155 nm [see Fig. 4(d)], we explored more investigations at these wavelengths. First, different VUV photon doses are exposed on the patterns before etching of NFC, and all the etch processes are performed. Figure 7 shows the comparison of poly-Si lines with different VUV photon doses at a wavelength of 155 nm. Line roughness significantly improved at a VUV photon dose of 3×10^{17} photons/cm^2. The LER reduced to 4.2 nm [Fig. 7(a)] from 6.7 nm by exposing the sample to VUV photons at a dose of 3×10^{17} photons/cm^2. In contrast, LER improvement is not significant at a VUV photon dose of 5×10^{14} photons/cm^2 (LER = 7.4 nm, Figure 7(b), suggesting that a certain photon dose is required to improve LER.

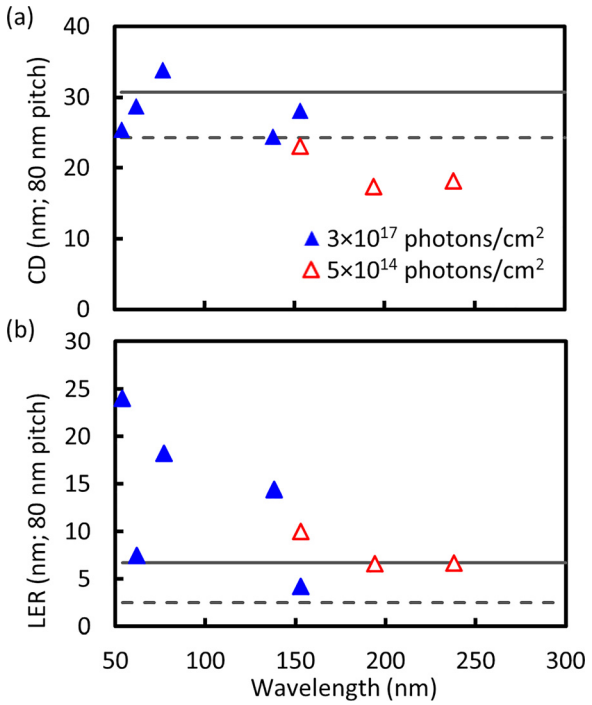

FIG. 5. (Color online) (a) Line CD and (b) LER of etched poly-Si lines at a pitch of 80 nm. VUV exposure was conducted prior to the NFC and poly-Si etch for this graph. Dotted line: CD or LER of e-beam patterned HSQ; solid line: CD or LER after poly-Si lines by the standard etch process without VUV treatment.

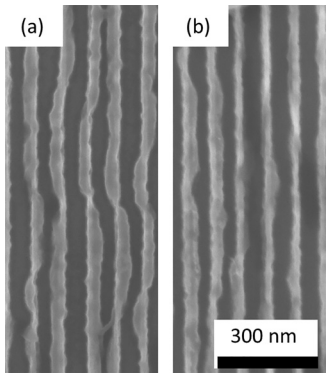

FIG. 6. Top-view of SEM images of poly-Si lines at a pitch of 80 nm. VUV photon (dose: 3×10^{17} photons/cm^2)-treated at wavelengths of (a) 54 nm (LER = 24.0 nm) and (b) 138 nm (LER = 14.4 nm). The process order is VUV/NFC/POLY.

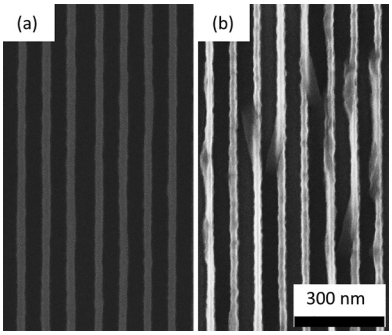

FIG. 7. SEM images of poly-Si lines at a pitch of 80 nm with a 155-nm VUV photon dose of (a) 3×10^{17} photons/cm^2 (CD = 28.1 nm and LER = 4.2 nm) and (b) 5×10^{14} photons/cm^2 (CD = 28.1 nm and LER = 7.4 nm). The process order is VUV/NFC/POLY.

We investigated the order of the etch and photon exposure process at a dose of 3×10^{17} photons/cm^2 for wavelengths of 62 and 155 nm. These wavelengths correspond to the absorption maxima of HSQ/NFC and NFC, respectively. Figures 8(a)–8(f) show SEM images of post-Si etch patterns at an 80 nm pitch with different process orders. For the NFC/VUV/POLY case [Figs. 8(a) and 8(d)], we first etched NFC and then exposed it to VUV photons followed by a poly-Si etch. CD and LER values were measured after each case and are plotted in Fig. 8(g). In the case of NFC/VUV/POLY at 62 nm [Fig. 8(a)], the poly-Si line collapsed and the measurement of CD and LER could not be performed. In cases of process order with NFC/VUV/POLY at a VUV photon dose of 3×10^{17} photons/cm^2, the patterns collapsed and CD/LER was not measurable at almost all the investigated wavelengths of 54, 62, 77, 88, and 112 nm. Although we are able to measure CD/LER on the samples treated at a wavelength of 155 nm, the LER becomes worse (10.4 nm) than the unexposed case (6.7 nm), as shown in Fig. 8(d). As shown in Fig. 5, when the VUV treatment was conducted before the etching of NFC, the LER is similar to or improved for both wavelengths of 62 nm [Fig. 8(b), LER = 7.5 nm] and 155 nm [Fig. 8(e), LER = 4.2 nm]. The process-order dependence might be attributed to the energy deposited on the narrow-patterned NFC lines and unetched NFC. Nest *et al.*[23] reported that no noticeable surface roughening occurred during VUV exposure on the blanket 193 photoresist, while a large loss of C=O and C–O–C bonds was observed. Different molecules and wavelengths were used in this work; however, we believe that similar modifications of molecules occurred during VUV exposure in this work. For patterned NFC (NFC/VUV/POLY), a deformation of the line-space patterns was observed. In the case of double-exposure (VUV treatment before and after NFC etch; VUV/NFC/VUV/POLY), line CD is similar to the unexposed case at a VUV wavelength of 62 nm, while the LER reduced down to 3.6 nm. NFC became resistive enough after the first VUV exposure to survive VUV exposure *after* etching of NFC. The second VUV exposure resulted in further improved LER. It was confirmed that for VUV exposure before patterning, NFC plays a critical role in the improvement of LER. In contrast, the smaller improvement of the LER was seen from 6.7 to 5.9 nm at a wavelength of 155 nm. The rougher line edge was observed compared with the VUV/NFC/POLY case (4.2 nm). These results suggest that the mechanism of LER reduction is different between 62 and 155 nm.

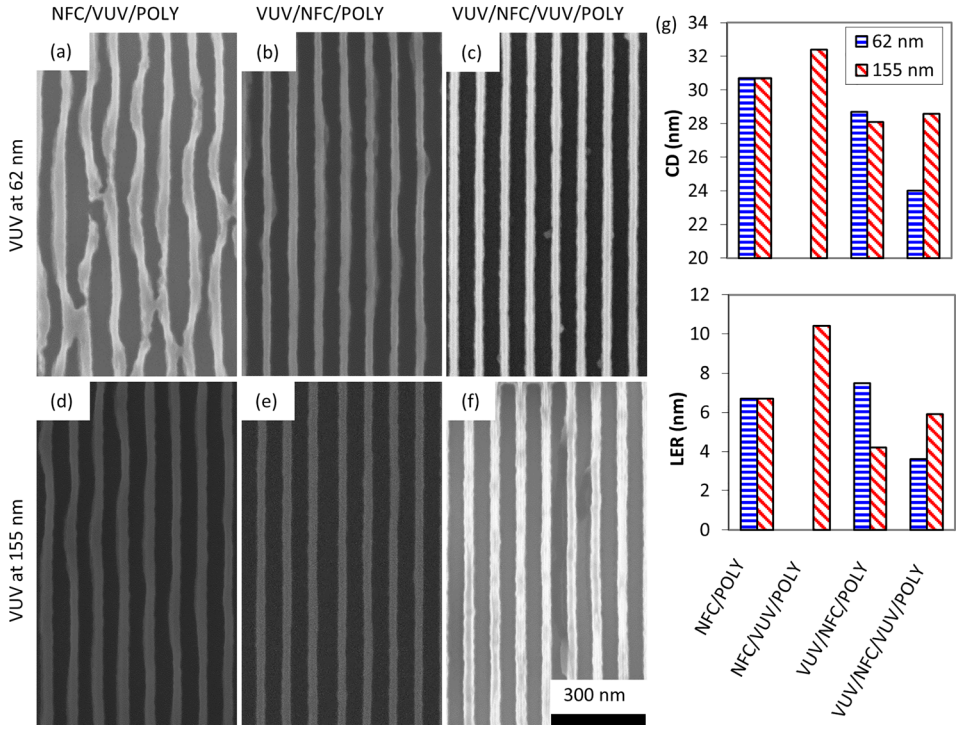

FIG. 8. (Color online) (a)–(f) SEM images of poly-Si lines with different process orders at VUV wavelengths of 62 and 155 nm. (g) Line CD and LER of each pattern. All the VUV photon exposure was conducted with a dose of 3×10^{17} photons/cm^2.

IV. SUMMARY AND CONCLUSIONS

The refraction indexes n and extinction coefficients k of HSQ and NFC were measured in the UV/VUV range using synchrotron radiation and ellipsometry. Based on these measurements, VUV/UV photons with different wavelengths were exposed to line space-patterns at a pitch of 80-nm to investigate the effect of VUV on line CD and LER of 50-nm thick poly-Si etching. No noticeable correlation in line CDs with extinction coefficients of HSQ and NFC was found. However, the LER depends on the wavelength, photon dose, and process order. The LER reduced from 6.7 nm for the unexposed case to 3.6 and 4.2 nm for VUV exposures at wavelengths of 62 and 155 nm, respectively. We also confirmed that a higher photon-dose results in better LER up to a dose of 3×10^{17} photons/cm^2. In contrast, a LER increase or pattern collapse was observed at other wavelengths such as 54, 77, and 138 nm. These results indicate that the improvement of LER by VUV/UV photon exposure is largely dominated by the energies and dose of the photons.

ACKNOWLEDGMENTS

VUV/UV exposure was carried out at the Synchrotron Radiation Center at the University of Wisconsin-Madison (UWM) and was supported by IBM and in part by the National Science Foundation under Grant No. CBET-1966231 and by the Semiconductor Research Corporation under Contract No. 2012-KJ-2349. Sample preparation and etch experiments were performed in the Micro Research Laboratory (MRL) at IBM T.J. Watson Research Center. The authors thank MRL management and staff for their contribution to this successful work.

[1]A. Asenov, S. Kaya, and A. R. Brown, IEEE Trans. Electron Devices **50**, 1254 (2003).
[2]F.-L. Yang, J.-R. Hwang, and Y. Li, *IEEE Custom Integrated Circuits Conference* (2006), p. 691.
[3]W. Steinhögl, G. Schindler, G. Steinlesberger, M. Traving, and M. Engelhardt, J. Appl. Phys. **97**, 023706 (2005).
[4]S. Burns *et al.*, Proc. SPIE **6153**, 61530K (2006).
[5]H.-Y. Tsai *et al.*, J. Vac. Sci. Technol., B **30**, 06F205 (2012).
[6]I. Sakai, J. Abe, H. Hayashi, Y. Taniguchi, H. Kato, Y. Onishi, and T. Ohiwa, Jpn. J. Appl. Phys., Part 1 **46**, 4286 (2007).
[7]Y. Seino *et al.*, Proc. SPIE **6923**, 69232O (2008).
[8]M. A. Guillorn *et al.*, J. Vac. Sci. Technol., B **27**, 2588 (2009).
[9]M. Glodde *et al.*, Proc. SPIE **7972**, 797216 (2011).
[10]G. Wakamatsu *et al.*, Proc. SPIE **8325**, 83250T (2012).
[11]J. Kim, Y. S. Chae, W. S. Lee, J. W. Shon, C. J. Kang, W. S. Han, and J. T. Moon, J. Vac. Sci. Technol., B **21**, 790 (2003).
[12]N. Kofuji and H. Miura, Appl. Phys. Express **2**, 106501 (2009).
[13]N. Kofuji and H. Miura, Jpn. J. Appl. Phys. **49**, 04DA23 (2010).
[14]S. U. Engelmann *et al.*, Proc. SPIE **8328**, 83280B (2012).
[15]M.-C. Kim, D. Shamiryan, Y. Jung, W. Boullart, C.-J. Kangand, and H.-K. Cho, J. Vac. Sci. Technol., B **24**, 2645 (2006).
[16]E. Pargon, K. Menguelti, M. Martin, A. Bazin, O. Chaix-Pluchery, C. Sourd, S. Drrough, T. Lill, and O. Joubert, J. Appl. Phys. **105**, 094902 (2009).
[17]E. Pargon, L. Azarnouche, M. Fouchier, K. Menguelti, R. Tiron, C. Sourd, and O. Joubert, Plasma Processes Polym. **8**, 1184 (2011).
[18]M. Brihoum, R. Ramos, K. Menguelti, G. Cunge, E. Pargon, and O. Joubert, J. Appl. Phys. **113**, 013302 (2013).
[19]L. Azarnouche, E. Pargon, K. Menguelti, M. Fouchier, O. Joubert, P. Gourand, and C. Verove, J. Vac. Sci. Technol., B **31**, 012205 (2013).
[20]M. Fouchier and E. Pargon, J. Appl. Phys. **115**, 074901 (2014).
[21]F. Weinboeck, D. Metzler, N. Kumar, G. S. Oehrlein, R. L. Bruce, S. Engelmann, and N. Fuller, Appl. Phys. Lett. **99**, 261501 (2011).
[22]D. Metzler, F. Weilnboeck, S. U. Engelmann, R. L. Bruce, and G. S. Oehrlein, J. Vac. Sci. Technol., B **34**, 041604 (2016).
[23]D. Nest *et al.*, Plasma Processes Polym. **6**, 649 (2009).
[24]Y. Ono *et al.*, Proc. SPIE **6519**, 65192O (2007).
[25]H. Miyazoe, S. U. Engelmann, M. A. Guillorn, D. Pei, W. Li, J. L. Lauer, D. B. Straight, J. L. Shohet, and N. C. M. Fuller, "Impact of vacuum ultraviolet exposure for the tight pitch patterning of poly silicon" (unpublished).
[26]"NIST atomic spectra database lines database," http://physics.nist.gov/PhysRefData/ASD/lines_form.html.
[27]H. Sinha *et al.*, J. Vac. Sci. Technol., A **28**, 1316 (2010).
[28]M. J. Rooks, N. Belic, E. Kratschmer, and R. Viswanathan, J. Vac. Sci. Technol., B **23**, 2769 (2005).
[29]D. Roessler, Br. J. Appl. Phys. **16**, 1119 (1965).
[30]D. E. Aspenes and A. A. Studna, Phys. Rev. B **27**, 985 (1983).
[31]M. J. Loboda and G. A. Toskey, Solid State Technol. **41**, 99 (1998), available at http://www.felcomllc.com/uploads/SolidStateTecharticleDC19982.pdf.
[32]J. Lee and D. B. Graves, J. Phys. D: Appl. Phys. **43**, 425201 (2010).